Mechanism for Cyclization Reaction by Clavaminic Acid Synthase. Insights from Modeling Studies†

Tomasz Borowski,*,‡ Sven de Marothy,§ Ewa Broclawik,‡ Christopher J. Schofield,|| and Per E. M. Siegbahn§

Institute of Catalysis and Surface Chemistry, Polish Academy of Sciences, ul. Niezapominajek 8, 30-239, Cracow, Poland, Department of Physics, Stockholm Center for Physics, Astronomy and Biotechnology, Stockholm University, S-106 91, Stockholm, Sweden, and Department of Chemistry, University of Oxford, Oxford OX1 3TA, U.K.

Received November 29, 2006; Revised Manuscript Received January 26, 2007

ABSTRACT: The mechanism of the oxidative cyclization reaction catalyzed by clavaminic acid synthase (CAS) was studied *in silico*. First, a classical molecular dynamics (MD) simulation was performed to obtain a realistic structure of the CAS-Fe(IV)═O-succinate-substrate complex; then potential of mean force (PMF) was calculated to assess the feasibility of the β-lactam ring, more specifically its C4′ corner, approaching the oxo atom. Based on the MD structure, a relatively large model of the active site region was selected and used in the B3LYP investigation of the reaction mechanism. The computational results suggest that once the oxoferryl species is formed, the oxidative cyclization catalyzed by CAS most likely involves either a mechanism involving C4′(*S*)−H bond cleavage of the monocyclic β-lactam ring, or a biosynthetically unprecedented mechanism comprising (1) oxidation of the hydroxyl group of PCA to an O-radical, (2) retro-aldol-like decomposition of the O-radical to an aldehyde and a C-centered radical, which is stabilized by the captodative effect, (3) abstraction of a hydrogen atom from the C4′(*S*) position of the C-centered radical by the Fe(III)−OH species yielding an azomethine ylide, and (4) 1,3-dipolar cycloaddition to the ylide with aldehyde acting as a dipolarophile. Precedent for the new proposed mechanism comes from the reported synthesis of oxapenams via 1,3-dipolar cycloaddition reactions of aldehydes and ketones.

Clavaminic acid synthase (CAS[1]) is a remarkable non-heme iron dioxygenase that catalyzes three separate oxidative reactions in the biosynthesis of clavulanic acid, a clinically used inhibitor of serine β-lactamases (*1*−*3*). Notably, all three oxidative reactions (Scheme 1), i.e. hydroxylation, cyclization, and desaturation, take place at the single active site of CAS (*4*), which in the native state hosts a single high-spin ferrous ion coordinated by the 2-histidine-1-carboxylate binding motif (*5*, *6*) and three water molecules (*7*). CAS belongs to a large superfamily of 2-oxoglutarate (2-OG) dependent oxygenases, a group of mononuclear non-heme iron enzymes that couples the oxidative decarboxylation of the 2-oxoglutarate cosubstrate to the 2-electron oxidation of a primary organic substrate (*8*, *9*). Based on numerous experimental and computational studies a generic catalytic reaction scheme for 2-OG dependent enzymes has been proposed, see Scheme 2. The cosubstrate (2-OG) first binds

Scheme 1: Three Oxidative Reactions Catalyzed by CAS

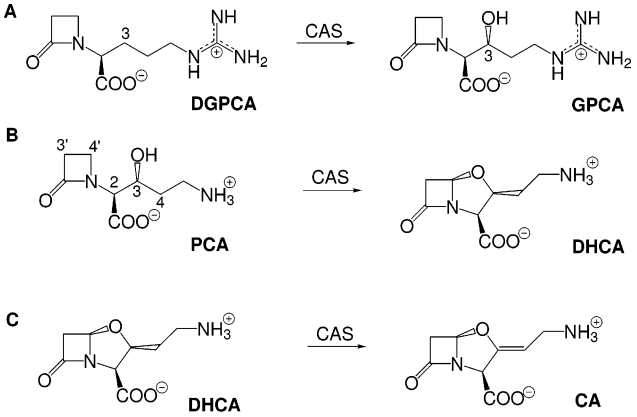

to the active site and coordinates the ferrous ion via its 1-carboxylate and 2-oxo groups (**A**) (*10*). Subsequent binding of the primary organic substrate (**A** → **B**) displaces the remaining water ligand from the Fe(II) coordination sphere, thus enabling the active site to bind dioxygen (**B** → **C**) (*11*, *12*). Once all required reactants are bound, the oxidative decarboxylation of 2-OG produces the complex **D**, where the primary organic substrate is positioned in the proximity of the Fe(IV)═O group, which has a high-spin, i.e., quintet, ground state (*13*−*18*). The oxidative power of the Fe(IV)═O intermediate is used to convert the organic substrate to the product (**D** → **E**), and the release of products (**E** → **A**) closes the catalytic cycle.

† This work was sponsored by the Polish State Committee for Scientific Research, Grant No. 2 P04A 042 26 to T.B. and E.B.

* Corresponding author. Tel: +48 12 6395158. Fax: +48 12 4251923. E-mail: ncborows@cyf-kr.edu.pl.

‡ Polish Academy of Sciences.

§ Stockholm University.

|| University of Oxford.

[1] Abbreviations: B3LYP, Becke's three parameter exchange-correlation potential; CA, clavaminic acid; CAS, clavaminic acid synthase; DFT, density functional theory; DGPCA, deoxyguanidinoproclavaminic acid; DHCA, dihydroclavaminic acid; KIE, kinetic isotope effect; MD, molecular dynamics; NAA, *N*-α-L-acetylarginine; PCA, proclavaminic acid; PDB, Protein Data Bank; PMF, potential of mean force; TS, transition structure; vdW, van der Waals; 2-OG, 2-oxoglutarate.

10.1021/bi602458m CCC: $37.00
Published on Web 02/27/2007

Scheme 2: The Generic Reaction Scheme for 2-Oxoglutarate Dependent Oxygenases

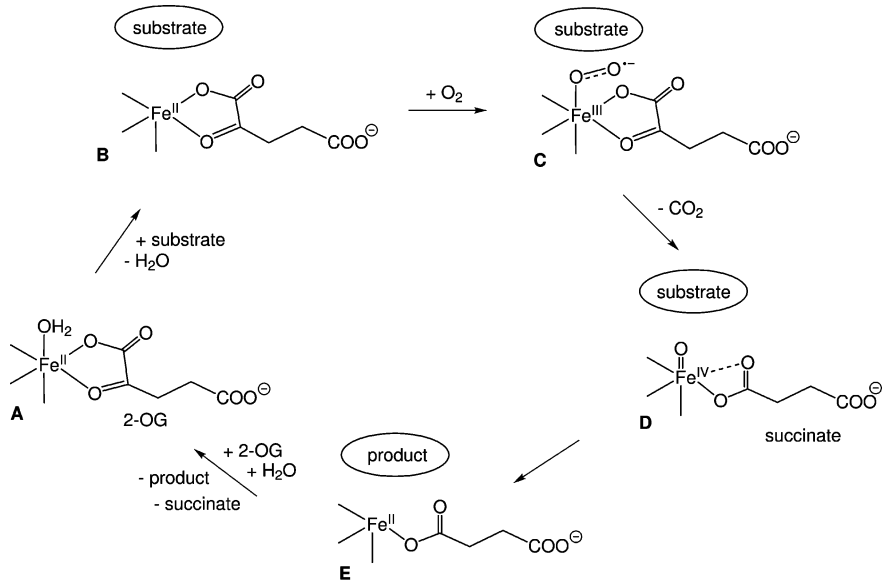

Taking into account the product specificity of the three different types of oxidative reaction catalyzed by CAS—hydroxylation, oxidative bicyclization, and desaturation—coupled to the high reactivity of the Fe(IV)═O group, an important question is raised as to how product specificity is achieved: How does CAS ensure that only one type of oxidative reaction occurs with very closely related substrates? With respect to this issue, important insights were gained from X-ray structures solved for CAS-Fe(II)-2-OG-substrate complexes (the intermediate **B** in Scheme 2) (*7*). In the structure with *N*-α-L-acetylarginine (NAA), an acyclic substrate analogue of deoxyguanidinoproclavaminic acid (DGPCA; PDB entry: 1DRY) that is similarly hydroxylated by CAS, the guanidino group of NAA interacts electrostatically with Asp202 and Asp233, whereas the carboxylate of NAA binds to Arg297 and the backbone NH of Ser134 (Figure 1A). Such a binding mode ensures that the 3-*pro*-*R* C−H bond of NAA, which is oxidized (*19*), projects toward the water ligand bound to Fe(II) trans to His279 (C−O distance of 2.4 Å). This, in turn, supports the proposal that the ferryl oxygen is also bound at this site (opposite to His279, approximate distance between the oxo atom and the 3(*R*) hydrogen is 1.9 Å; see inset in Figure 1A), at least just before substrate oxidation, because it might be originally formed trans to His144 (*20*). However, a crystal structure with proclavaminic acid (PCA), the substrate for the cyclization reaction (PDB entry: 1DRT; Figure 1B), is less informative concerning the mechanism of the intriguing oxidative cyclization. As shown in Figure 1B, Arg297 is positioned to form electrostatic interaction and hydrogen bond with the carboxylate and hydroxyl group of PCA, respectively. Arg115 is also quite close to the carboxylate of PCA. Ser134 forms, through its side chain hydroxyl, a hydrogen bond with the hydroxyl of PCA. The amino end of PCA is rather far from the carboxyl groups of Asp202 and Asp233 (N−O distance of 3.9 and 5.1 Å, respectively), and instead, forms a hydrogen bond with the backbone carbonyl of Leu132 (not shown). Notably, the distance between iron and the C4′ carbon is rather large (5.44 Å), which leads to an approximate distance of 3.4 Å between the C4′(*S*) hydrogen and the oxo atom (see inset in Figure 1B). On the other hand, a short hydrogen bond between the oxo atom and the hydroxide group of PCA is anticipated. However, one might suspect that in the reactive complex **D** (Scheme 2), due to the presence of the Fe(IV)═O group, the binding interactions between PCA and CAS could be somewhat different than in 1DRT (**B** in Scheme 2).

Concerning the mechanism of the oxidative cyclization catalyzed by CAS (Scheme 1B), isotope labeling studies have provided valuable insights: oxygen atom of the 5-membered ring of dihydroclavaminic acid (DHCA) was shown to derive exclusively from the C3-bound hydroxyl of PCA, and the C2−H and C3′−H bonds are not cleaved during the cyclization or desaturation reactions (*22*). DHCA was identified as an intermediate, and its stereochemistry has been confirmed (*23*). Studies with stereospecifically deuterated PCA at C4′ showed that the C4′(*S*) hydrogen is specifically lost, while the C4′(*R*) hydrogen is retained during the oxidative cyclization (*24*). Experiments using PCA with tritium labels bound to C4′ and C3 unambiguously showed that the cyclization reaction precedes desaturation, and a substantial kinetic isotope effect (KIE) was measured for C4′-labeled PCA (primary $^{T}(V/K) = 11.9 \pm 1.7$) indicating that the C4′(*S*)−H bond cleavage contributes to the rate-limiting step (*25*). Finally, a β-secondary KIE was measured, but the results of these studies did not allow for discrimination between a possible radical and cationic nature of the species at the C4′ carbon in the intermediate formed by the C4′−H bond cleavage (*26*).

Based on these isotope labeling studies and the crystal structure of the CAS-Fe(II)-2-OG-PCA complex a mechanism presented in Scheme 3 was proposed for the oxidative cyclization catalyzed by CAS (*7*, *26*). The oxoferryl species abstracts the C4′(*S*) hydrogen, which leads to species **b** with Fe(III)−OH and the C4′-centered radical. An attack of the C3-bound hydroxyl at C4′ coupled with hydrogen atom transfer to Fe(III)−OH leads to the product complex **d**, with Fe(II)−OH_2 and DHCA. Alternatively, an electron transfer from the C4′ radical to Fe(III)−OH affords species **c** with an imminium ion and a Fe(II)−OH complex. An attack of the C3-bound hydroxyl at the C4′ cation coupled with a

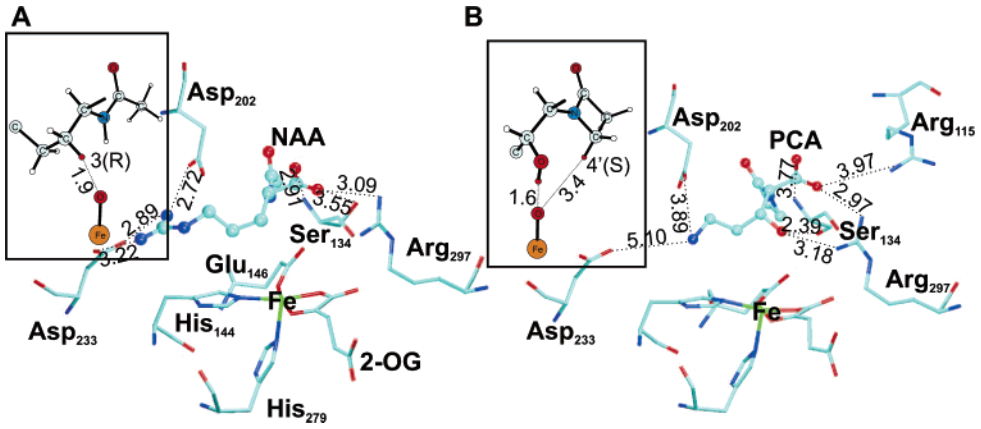

FIGURE 1: Views from the X-ray crystal structures of active site regions in CAS-Fe(II)-2-OG-substrate complexes. (A) Complex with a substrate for hydroxylation reaction (NAA); 1DRY. (B) Complex with PCA-substrate for the oxidative cyclization; 1DRT. Insets present important distances between the oxo atom and hydrogens from the substrates (added at their standard positions). Note that the oxo atom was added only for illustrative reasons, since the crystal structures were solved for the resting Fe(II) states, which lack the oxo group. Figure produced with VMD (*21*).

Scheme 3: The Experimentally Suggested Mechanism for Oxidative Cyclization Catalyzed by CAS

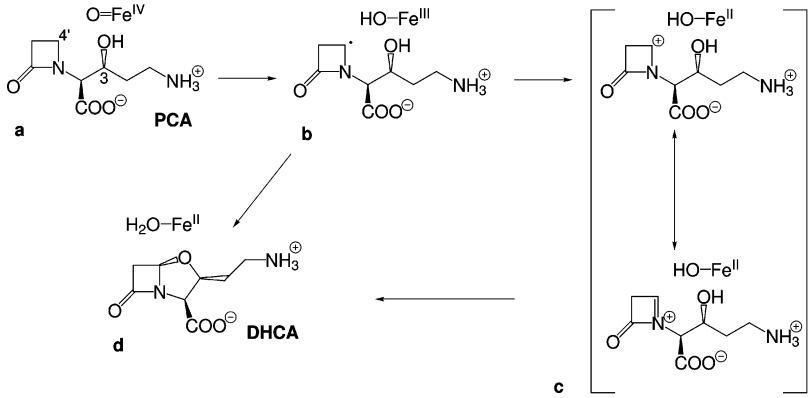

proton transfer to Fe(II)−OH converts species **c** into the product complex **d**.

Taking into account the large distance between C4′ and iron in the crystal structure of the CAS-Fe(II)-2-OG-PCA complex (1DRT) it was important to test if the mechanism presented in Scheme 3 is viable. To this end the following modeling studies were done: (1) classical molecular dynamics simulation for the CAS-Fe(IV)═O-succinate-PCA complex, (2) calculation of classical potential of mean force (PMF) for the β-lactam ring, pulled by the C4′(*S*) hydrogen, approaching the oxo atom, and (3) B3LYP calculations for plausible mechanisms of oxidative cyclization. Although a mechanism involving C4′−H bond cleavage cannot be eliminated, the results of these investigations suggest that a novel mechanism, involving 1,3-dipolar cycloaddition, could be responsible for the oxidative cyclization by CAS.

1. COMPUTATIONAL DETAILS

The setup and parameters used for classical dynamics simulations are described in the Supporting Information. All classical MD calculations were done with the AMBER 8 suite of programs (*27*).

DFT Models and Methods. The quantum chemical model of the active site region in the CAS-Fe(IV)═O-succinate-PCA complex was based on the averaged structure (500 snapshots (#1100−1600) corresponding to a 0.5 ns time range) from the 2 ns production MD simulation. The model, which consists of 135 atoms (Figure 2), comprises the following groups: PCA, Fe═O, two methylimidazoles (His144, His279), three acetates (succinate, Asp202, Asp233), propionate (Glu146), two methanols (Tyr149, Tyr299), methylguanidine (Arg297), $CH_3CONHCH_2CH_2OH$ (Ser133−Ser134 peptide bond and Ser134 side chain), and three water molecules solvating Asp202 and Asp233. Several terminal atoms, marked with asterisks in Figure 2, were constrained to their positions in the averaged MD structure. The total charge of the quantum chemical model is −1, and the spin state is quintet.

All quantum chemical calculations employing this model were performed with hybrid DFT. The B3LYP exchange-correlation functional (*28*, *29*) in the Jaguar (*30*) program was used. Geometry optimizations were done with a valence double-ζ basis set coupled with an effective core potential describing the innermost electrons on iron. This particular basis set is labeled lacvp in Jaguar. For the optimized structures the electronic energy was computed with a bigger basis set of triple-ζ quality with polarization functions on all atoms except iron (lacv3p for iron and cc-pVTZ(-f) for the other atoms). The solvent corrections were calculated for the first barriers of the two mechanisms with the self-consistent reaction field method implemented in Jaguar (*31*, *32*). A dielectric constant of 4 and a probe radius of 1.4 Å were used to model the protein surroundings of the active site. Due to the size of the system, only approximate

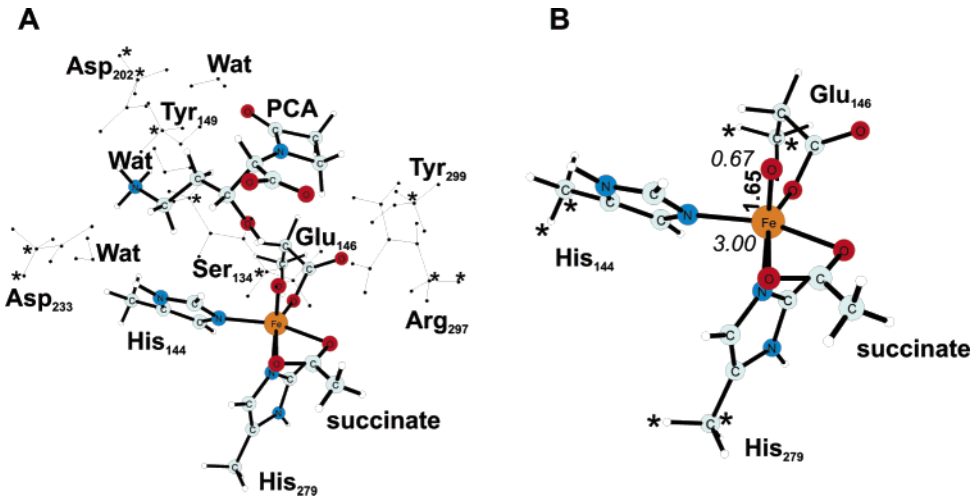

FIGURE 2: The optimized structure for the QM model for the active site region in the CAS-Fe(IV)═O-succinate-PCA complex. (A) PCA and iron with its ligands are displayed as balls-and-sticks, whereas the second-shell residues are simplified. (B) The second-shell residues are omitted. Distances in Å are in bold, spin populations are in italics, and atoms marked with asterisks were constrained to their positions in the averaged MD structure.

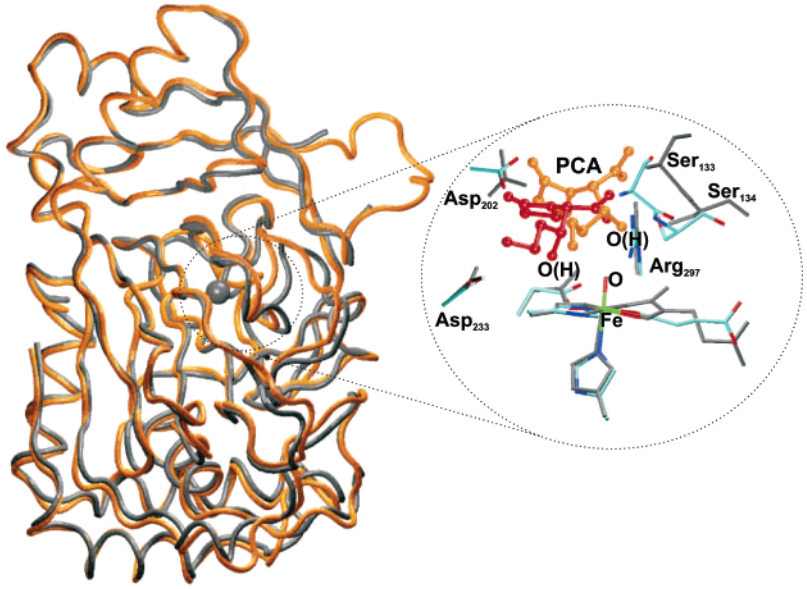

FIGURE 3: Superimposed structures from the 1DRT crystal structure and snapshot #1350 from the MD simulation. On the left the backbone atoms are presented; 1DRT in gray, snapshot in orange. On the right, the superimposed active site regions are shown. Crystal structure in gray, MD snapshot with atom-type colors. PCA from 1DRT in orange, PCA from the MD snapshot in red. Note the difference in the conformations of Ser133 and Ser134 and the position of hydroxyl group of PCA. Figure produced with VMD (*21*).

transition structures (TS) were optimized. For selected approximate reaction coordinates (interatomic distances) relaxed scans were performed with a step of 0.1 Å for bonds not involving hydrogens and 0.05 Å for X−H distances. Once the maximum energy point (approximate TS) was found, optimizations starting from two points on both sides of the maximum and 0.1 Å away from the TS were performed in order to check if the TS found connects the right substrate and product. For the 1,3-dipolar cycloaddition reaction, a two-dimensional variant of this procedure was used to find the approximate saddle point.

2. RESULTS

MD Structure of the CAS-Fe(IV)═O-succinate-PCA Complex. The overall structure of the protein backbone during the MD simulation remained very similar to that in the crystal structure (1DRT), see Figure 3. The calculated root-mean-square-deviation (rmsd) to the starting structure (1DRT) for the backbone atoms does not exceed 1.4 Å (see Figure S3 in Supporting Information). However, in the active site region, there are some important changes (Figure 3). First, the hydroxyl group of PCA forms a hydrogen bond with the iron−oxo oxygen and no longer interacts with Ser134. Second, the amino group of PCA interacts ionically and via hydrogen bonds with Asp202 and Asp233. Moreover, the carboxyl group of PCA forms a salt-bridge with Arg297, loses its interaction with Arg115, and forms hydrogen bonds with backbone nitrogen and side-chain hydroxyl of Ser134. Figure 3 reveals that the X-ray and MD structures overlap well except for the substrate (PCA) and the Ser133−Ser134 fragment. Interestingly, these two serines are a part of a loop, and the observed mobility of this fragment may have functional relevance, e.g., in induced fit during substrate binding. In summary, the binding situation of the ionic

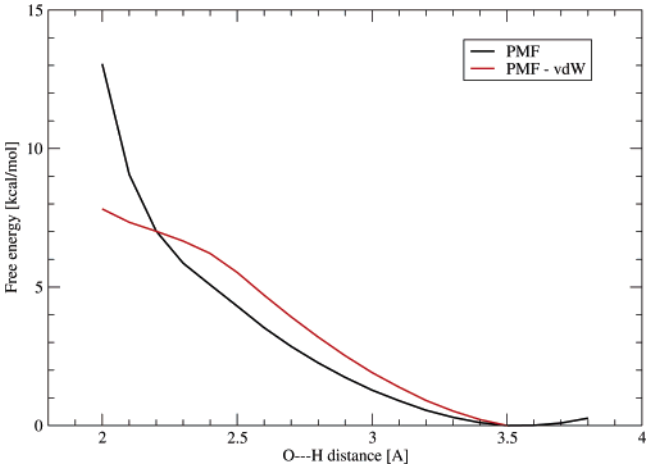

FIGURE 4: The calculated classical PMF for the C4′(*S*) hydrogen of PCA approaching the oxo atom of the Fe(IV)═O core (PMF), and the difference between the PMF and the classical interaction energy between the L_4Fe(IV)═O complex and the probe molecule representing the C4′-H moiety (PMF-vdW).

groups of PCA in the MD structure resembles largely the substrate−enzyme interactions in the 1DRY crystal structure (Figure 1A). With respect to the oxidative cyclization, the distance between the hydrogen atom from the hydroxyl group of PCA and the oxo atom remains short (average 1.86 Å) throughout the 2 ns simulation, whereas the separation between the oxo atom and the C4′(*S*) hydrogen stays rather large, with an average of 3.77 Å (Figure S4 in Supporting Information). Moreover, the (PCA)O-H−O(oxo) angle is large (average of 157 deg, Figure S5 in Supporting Information), which together with the short H−O(oxo) distance indicates that a H-bond forms between the hydroxyl group of PCA and the oxo oxygen.

PMF for the β-Lactam Ring Approaching Fe(IV)═O. The classical potential of mean force (PMF) was calculated for the β-lactam ring of PCA approaching the oxo atom of the Fe(IV)═O core. More specifically, the distance between the 4′(*S*) hydrogen and the oxo atom was selected as a coordinate scanned in these calculations. The purpose was to estimate the free energy cost for such a motion, which should be expected to take place if the C4′−H bond were to be cleaved by the Fe(IV)═O species. The calculated PMF and the difference between PMF and the estimated vdW (and electrostatic) interaction between the Fe(IV)═O species and the C4′-H group are presented in Figure 4. In the 3.5 → 2.0 Å range the PMF is uniformly repulsive, which means that the structure observed in the 2 ns MD simulation is optimal with respect to changes in this coordinate. Moreover, the interactions other than the C4′-H−O═Fe(IV)(L) vdW and electrostatics also give a repulsive curve (PMF − vdW in Figure 4), and the estimated free energy cost for C4′(*S*) hydrogen getting at 2 Å from the oxo atom is 7.8 kcal/mol.

DFT: C−H Bond Activation and Following Steps. The mechanisms considered in this work are presented in Scheme 4, whereas the calculated energy profiles are shown in Figure 5.

The previously proposed mechanism deriving from experimental observations (Scheme 4) involves, as a first step, the abstraction of the C4′(*S*) hydrogen atom by the Fe(IV)═O (**a** → **b**). This process proceeds through transition structure $\mathbf{TS}_{C4-H}$ (Figure 6A) and involves a calculated activation energy barrier of 21.4 kcal/mol (21.8 kcal/mol with the dielectric solvent effects included). $\mathbf{TS}_{C4-H}$ is characterized by a rather short distance between the oxo oxygen and the C4′(*S*) hydrogen atom (1.38 Å), with the C4′(*S*)−H bond substantially elongated (1.21 Å). The spin population on C4′ (−0.24) predicts that a radical with beta spin forms in this reaction. Indeed, both the structure and spin populations calculated for the product **b** (Figure 6B) indicate that it has a radical center at C4′ with beta spin, whereas the five unpaired electrons of the high-spin iron have alpha spin. In intermediate **b** the distance between C4′ and the C3-bound

Scheme 4: The Mechanisms for Cyclization Reaction by CAS Considered in This Work

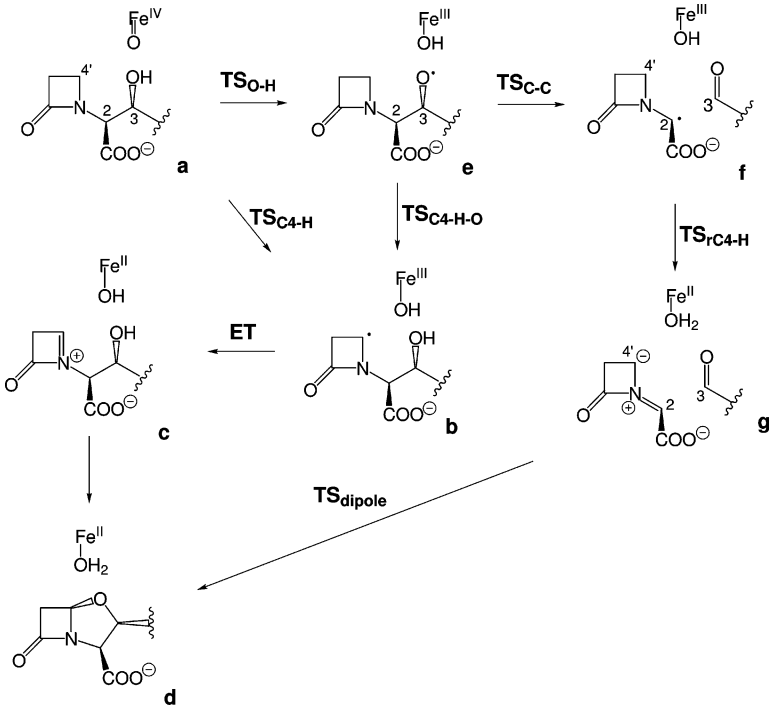

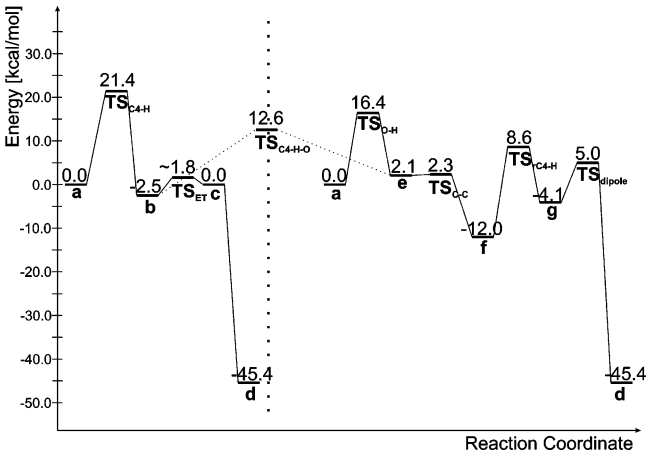

FIGURE 5: The calculated energy profiles along the reaction paths presented in Scheme 4. Left: The experimentally suggested mechanism. Right: The mechanism suggested in this work.

oxygen is 3.19 Å, whereas the distance between the iron-bound hydroxyl oxygen and the hydrogen from the C3-bound OH group is 1.67 Å.

A slightly endothermic (by 2.5 kcal/mol) electron transfer (ET) from C4′ to Fe(III) leads from species **b** to an imminium cation intermediate **c**. This ET leads to elongation of the Fe−OH bond (from 1.85 to 2.04 Å), noticeable C4′-N bond shortening (from 1.42 to 1.33 Å), and most notably, a substantial decrease in the distance between the Fe-bound hydroxide oxygen and the hydrogen atom of the C3-bound OH group (from 1.67 to 1.28 Å). This last feature suggests that the proton transfer from the C3-bound OH group in the imminium cation species to the Fe(II)-bound hydroxide should be an easy process. In fact, intermediate **c** was found to undergo a spontaneous proton transfer and ring closure leading to the final product complex **d**, and the C4′−O(C3) distance had to be constrained during the geometry optimization of **c** in order to prevent this spontaneous process. Attempts to optimize the TS structure with the large model failed, but the small model (without the second-shell residues and ionic groups of PCA, see Supporting Information) gave a barrier of 4.3 kcal/mol. From the comparison of structures of $\mathbf{b}_{small}$ and $\mathbf{TS}_{ETsmall}$ and the character of the imaginary frequency mode, it follows that several (at least 5) internal coordinates have similarly large contributions to the reaction coordinate, and due to the multidimensional character of this process, the TS could not be located for the large model. Nevertheless, the barrier for cyclization (**b** → **d**) was estimated to be small (around 4.3 kcal/mol), which indicates an efficient process.

The spin population on iron in species **c** and **d** is consistent with a high-spin ferrous state of the metal. The proton transfer and ring closure leading from **c** to **d** is highly exothermic (45.4 kcal/mol), and thus, irreversible.

DFT: O−H Bond Activation and Following Steps. An alternative reaction mechanism starts with oxidation of the C3-bound hydroxyl to an oxygen radical species **e** (Scheme 4). This process involves an activation energy of 16.4 kcal/mol (18.0 kcal/mol with the solvent dielectric contributions) connected with transition structure $\mathbf{TS}_{O-H}$ presented in Figure 7A. From spin populations it is apparent that, as for $\mathbf{TS}_{C4-H}$, the substrate radical produced in this step has beta spin, whereas the high-spin ferric ion has five unpaired electrons with an alpha spin. This spin population is indeed found for the radical intermediate **e** presented in Figure 7B. The oxygen radical intermediate (**e**) is calculated to be 2.1 kcal/mol less stable than the reactant complex **a** (Figure 5).

In intermediate **e** the beta spin of the oxygen radical is somewhat delocalized; the spin populations on oxygen, carbon C2, nitrogen, and the carbonyl oxygen in the β-lactam ring are −0.72, −0.17, −0.02, and −0.03, respectively. Moreover, the C2−C3 bond is markedly elongated compared to the reactant complex **a** (from 1.57 to 1.66 Å), which, together with the spin delocalization, indicates that the C2−C3 bond in **e** is activated for homolytic cleavage. This observation was confirmed by finding a transition structure for that C−C bond scission ($\mathbf{TS}_{C-C}$), whose energy is only 0.2 kcal/mol higher than for intermediate **e**, indicating an extremely efficient cleavage. From the spin populations calculated for $\mathbf{TS}_{C-C}$ (Figure S7) and **f** it is easy to recognize that during the C−C bond cleavage the radical character is transferred from the C3 oxygen to the carbon C2 with the C3 carbon becoming a part of an aldehyde group. The substantial stability of **f** with respect to **e** (14.1 kcal/mol energy difference; Figure 5) comes, at least in part, from the captodative effect stabilizing the carbon centered radical with neighboring electron-donating (COO^-) and electron-withdrawing (lactam) groups (*33*). This effect is manifested also in delocalization of beta spin from carbon C2 onto these groups (Figure 7C).

Once the radical intermediate **f** is formed, the progress of the catalytic reaction requires a hydrogen atom abstraction from the C4′(*S*) position, a process leading to intermediate **g** with azomethine ylide and aldehyde fragments. This reaction involves an activation barrier of 20.6 kcal/mol involving a transition structure $\mathbf{TS}_{rC4-H}$ presented in Figure 8A. It seems important to note here that $\mathbf{TS}_{rC4-H}$ connects intermediates **g** and **f2**, where the latter is a substrate imminum ion/Fe(II)−OH species formed by an electron transfer from the substrate radical to iron in the radical intermediate **f**. The calculated energy of **f2** is −0.8 kcal/mol. Due to the technical difficulties the transition structure connecting **f** and **f2** has not been sought.

The spin populations shown in Figure 8B indicate that the ylide and aldehyde fragments have closed-shell electronic structures, whereas the ferrous ion is in the high-spin quintet state. The following cycloaddition reaction between these closed-shell species is a concerted process involving an activation energy of 9.1 kcal/mol and leading through a transition structure $\mathbf{TS}_{dipole}$ presented in Figure 8C. For $\mathbf{TS}_{dipole}$ the two critical distances between the atoms forming the two new bonds are 2.18 Å for C4′−O and 2.41 Å for C2−C3, whereas the carbonyl bond is elongated from 1.26 to 1.30 Å.

The two reaction mechanisms described above, one involving species **a**, **b**, **c**, and **d** and the second with intermediates **a**, **e**, **f**, **g**, and **d** (Scheme 4), are potentially interconnected by a transition structure for intramolecular hydrogen atom transfer, $\mathbf{TS}_{C4-H-O}$ (Figure S8). In this reaction a hydrogen atom is transferred between the C3-bound oxygen and the C4′ carbon, so intermediate **b** is transformed into **e** or vice versa. However, the activation energy for this process is markedly larger than for the

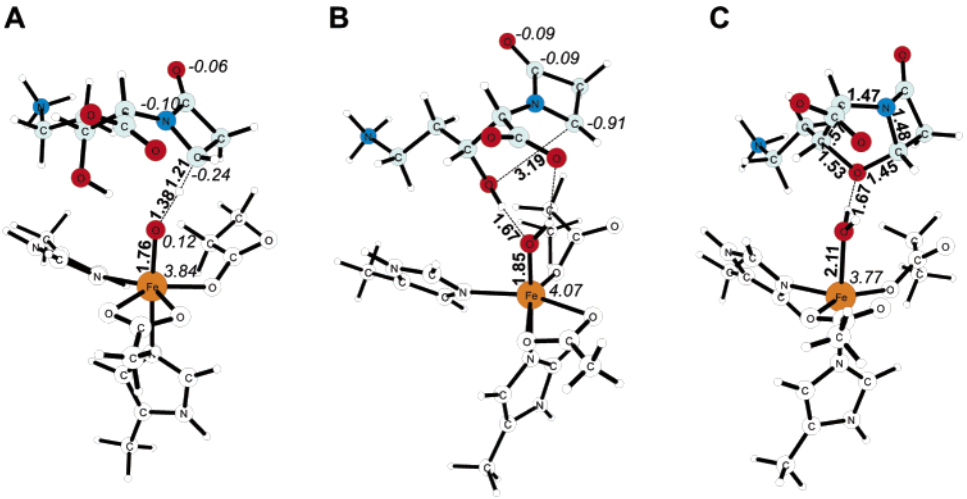

FIGURE 6: The optimized structures of (A) the transition structure for C4′−H bond cleavage by the Fe(IV)═O species, $\mathbf{TS}_{C4-H}$; (B) the intermediate with a radical center at C4′, **b**; and (C) the final cyclization product complex **d**. Second-shell residues are omitted for clarity. Distances are in bold, and spin populations are in italics.

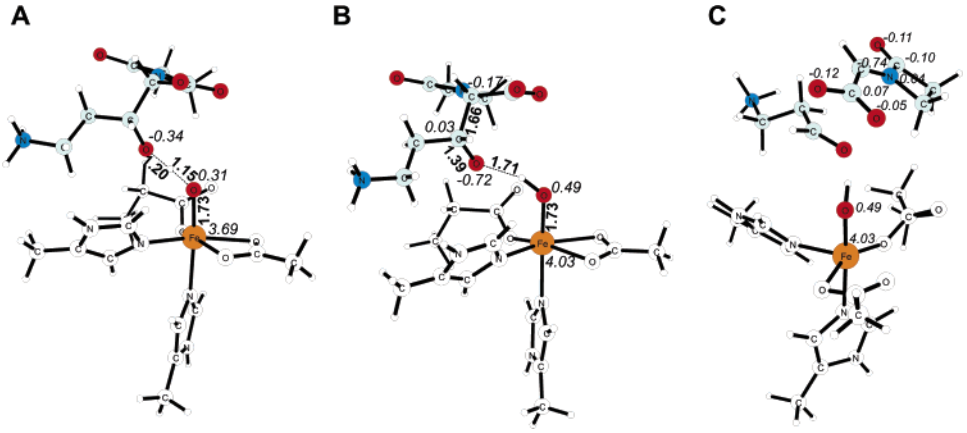

FIGURE 7: The optimized structures of (A) the transition structure for O−H bond cleavage by the Fe(IV)═O species $\mathbf{TS}_{O-H}$, (B) the O-radical intermediate **e**, and (C) the C-radical intermediate **f**. Second-shell residues are omitted for clarity. Distances are in bold, and spin populations are in italics.

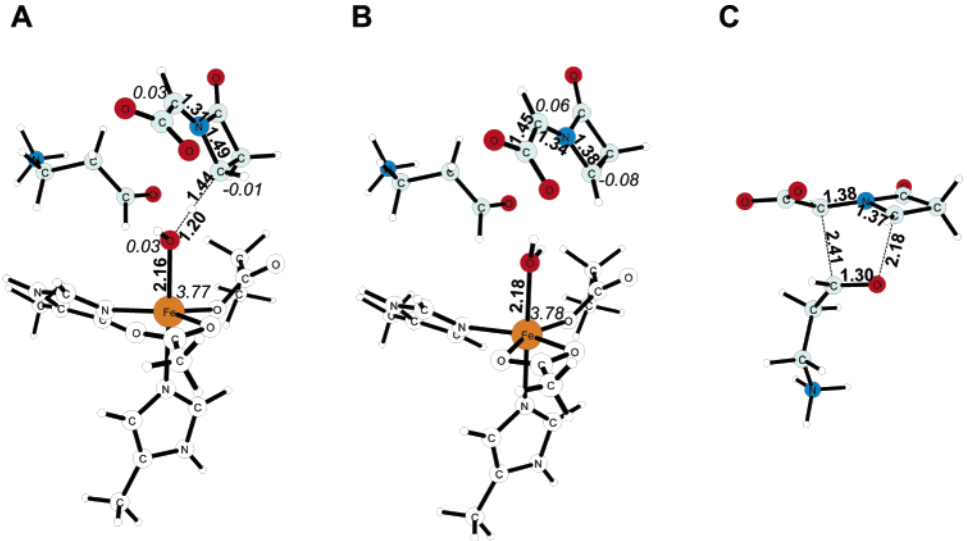

FIGURE 8: The optimized structures of (A) the transition structure for C4′(*S*)−H bond cleavage in the carbon radical species, $\mathbf{TS}_{rC4-H}$; (B) the ylide intermediate **g**; and (C) the transition structure for 1,3-dipolar cycloaddition of aldehyde to azomethine ylide $\mathbf{TS}_{dipole}$. Second-shell residues are omitted for clarity. Distances are in bold, and spin populations are in italics.

competing reactions of intermediates **b** and **e** (Figure 5). Importantly, from the energy profile (Figure 5) it follows that reactant **a** evolves preferentially (kinetic discrimination) into intermediate **f**, for which the fastest decay channel proceeds through $\mathbf{TS}_{rC4-H}$, **g**, and $\mathbf{TS}_{dipole}$. Transformation of **f** into **b** involves an accumulated barrier of 24.6 kcal/

mol, which is 4.0 kcal/mol larger than the barrier connected with $\mathbf{TS}_{rC4-H}$.

3. DISCUSSION

The reaction mechanism for the oxidative cyclization by clavaminic acid synthase has been studied with computational methods. The results presented above suggest that the biosynthesis of the oxapenam bicyclic structure could involve a 1,3-dipolar cycloaddition, which, to our knowledge, is a reaction unprecedented in enzymatic reactions.

The available crystal structure for the CAS-Fe(II)-2-OG-PCA complex (1DRT) provides only approximate information concerning the relative orientation of substrate (PCA) with respect to the reactive oxoferryl species. In this crystal structure the Fe−C4′ distance is 5.4 Å, whereas the hydroxyl oxygen of PCA is 4.2 Å away from iron. In the reactive complex **D** (Scheme 2), where the polar oxoferryl group is present, the binding mode of PCA could be somewhat different. This is indeed observed in the structure of intermediate **D** modeled with classical molecular dynamics simulation (Figure 3). In this structure the hydroxyl group of PCA is positioned to form a hydrogen bond with the oxo atom, and the charged amino group of PCA interacts with Asp202 and Asp233, whereas the carboxyl group of PCA forms hydrogen bonds and ionic interactions with Ser134 and Arg297. The average distances between iron and the hydroxyl oxygen and C4′ are 3.8 and 5.8 Å, respectively, which means a 0.4 Å difference for each of these distances with respect to the crystal structure 1DRT. Importantly, the preference for shorter contact between iron and the hydroxyl oxygen, compared to iron−C4′, already observed in the Fe(II) complex (1DRT; 1.2 Å difference), is further enhanced in the Fe(IV)═O intermediate (MD structure; 2.0 Å difference). Furthermore, the calculations of classical potential of mean force (PMF, Figure 4) show that convergence of the C4′(*S*) hydrogen and the oxo atom is a difficult process; shortening the distance to 2 Å is endergonic by at least 7.8 kcal/mol. Thus, both structural (X-ray, MD) and PMF data imply that the attack of oxoferryl species on C4′(*S*) hydrogen of PCA is most likely a difficult process. On the other hand, the hydroxyl group of PCA is positioned to form a strong hydrogen bond (1.8 Å) with the oxo oxygen, which makes this group a preferred candidate for the initial site of substrate oxidation. Thus, the energetics of two alternative mechanisms the for cyclization reaction by CAS (Scheme 4), one starting with the C4′(*S*)−H bond cleavage, the second with the O−H bond activation, were investigated with DFT methods (B3LYP) applied to a relatively large model of the active site region of the CAS-Fe(IV)═O-succinate-PCA complex (Figure 2).

The results of the DFT investigations confirm the conclusion drawn from structural and PMF data, namely, that in the first step of the oxidative cyclization of PCA the hydroxyl group is significantly better placed to be oxidize than the C4′ carbon (Figure 5). The calculated difference in activation energies is 5 kcal/mol in favor of O−H bond cleavage (3.8 kcal/mol with the dielectric solvent effects included).

From the energy profile presented on the left-hand side of Figure 5, one can notice that the rate-limiting step in the mechanism involving C4′(*S*)−H bond cleavage as a first step is the first hydrogen abstraction step itself with a calculated activation energy of 21.4 kcal/mol (21.8 with the solvent effects). The C4′ centered radical **b** (Scheme 4), produced in this reaction, can then be oxidized to the imminium cation **c** in a slightly endothermic process (2.5 kcal/mol) involving a barrier of 4.3 kcal/mol. Species **c** is unstable with respect to ring closure to the final product **d**, which means that the electron transfer producing the imminium ion and the ring closure are concerted processes.

The energy profile presented on the right-hand side of Figure 5 corresponds to a mechanism starting with oxidation of the hydroxyl group (Scheme 4). In this mechanism, the initial O−H bond cleavage is a relatively fast process, with calculated activation energy of 16.4 kcal/mol (18.0 kcal/mol with the solvent effects), leading to a short-lived oxygen-radical intermediate **e**. Species **e**, in a radical analogue of retro-aldol reaction, can decompose to an aldehyde and a C2-centered radical (**f**). This decomposition reaction is predicted to be very fast (activation energy of 0.2 kcal/mol), and it is exothermic by 14.1 kcal/mol, mostly due to the captodative effect stabilizing the C2-centered radical. Interestingly, the following step (**f** → **g**), which involves the C4′(*S*)−H bond activation by the Fe(III)−OH group, is predicted to be the rate-limiting step (calculated activation barrier of 20.6 kcal/mol). Thus in both mechanisms considered here the same bond (C4′(*S*)−H) is cleaved in the rate-limiting step. This, in turn, means that the two mechanisms provide equally good explanation for the available kinetic isotope effects (KIE) data (*25*, *26*), which suggest that C4′(*S*)−H cleavage contributes to the rate-limiting step. Once the azomethine ylide/aldehyde intermediate **g** is formed, the 1,3-dipolar cycloaddition reaction, with aldehyde as dipolarophile (calculated activation barrier of 9.1 kcal/mol), leads to the bicyclic product complex **d**. The low activation barrier calculated for this reaction agrees with the results of previous calculations, which show that azomethine ylide reacts readily with unsaturated compounds (*34*).

Interestingly, β-lactam based azomethine ylide reactivity has been used for synthesis of β-lactam antibiotics (*35*−*37*), and, most notably, aldehydes and ketones have been shown to act as dipolarophiles in cycloadditions leading to oxapenams (*38*). Further, support for the viability of the proposed mechanism comes from recent report that acetylcholinesterase can template the (unnatural) Huisgen 1,3-dipolar cycloaddition of azides and acetylenes to give 1,2,3-triazoles (*39*). Thus, the 1,3-dipolar cycloaddition step in the proposed reaction mechanism (**g** → **d** in Scheme 4) has experimental precedence. On the other hand, the two first steps of the reaction mechanism, i.e., O−H bond cleavage followed by C−C splitting (**a** → **e** and **e** → **f**), resemble a part of the mechanism proposed for enzymatic side-chain cleavage of cholesterol by cytochrome P-450 (*40*). Finally, the hydrogen atom abstraction from C4′ by Fe(III)−OH (**f** → **g**) resembles the first step of the catalytic reaction of lipoxygenase, where the Fe(III)−OH group abstracts a hydrogen atom from an activated (polyunsaturated) hydrocarbon (*41*). Notably, the cycloaddition reaction with aldehyde as dipolarophile proceeds regioselectively with oxapenams as the sole products (oxygen from aldehyde attacks exclusively C4′) (*38*). Calculations for a small model system, i.e., acetaldehyde and protonated (on the carboxylic group) ylide, gave barriers of 6.1 and 11.4 kcal/mol for the observed and reversed regioselectivities, respectively.

4. CONCLUSIONS

The results of the classical MD simulations suggest that the active site region of the CAS-Fe(IV)═O-succinate-PCA has a well-defined structure consistent with the concept of "negative catalysis" which proposes that enzymes with highly reactive intermediates achieve product selectivity via ablation of unproductive/undesirable pathways (*42*). Interestingly, in this structure the hydroxyl group of PCA lies substantially closer to the oxoferryl group than the C4′-bound hydrogen of PCA. Thus, this structure, together with a repulsive PMF calculated for an approach of 4′(*S*) hydrogen of PCA toward the oxo group, suggests that the alcohol group of PCA is oxidized first by the reactive oxoferryl species. The DFT investigations indeed show that oxidation of an alcohol group is markedly easier than activation of the C4′−H bond. Moreover, based on the DFT results, a novel mechanism is proposed for the cyclization reaction by CAS. This new mechanistic hypothesis involves O-radical fragmentation, ylide formation, and 1,3-dipolar cycloaddition with aldehyde as dipolarophile. Importantly, this new mechanism is consistent with the isotope kinetics data (*24*, *25*) and predicts formation of a relatively long-lived intermediate (**f**), whose accumulation might be experimentally verifiable.

ACKNOWLEDGMENT

T.B. thanks Dr. Marcin Król for many fruitful discussions.

SUPPORTING INFORMATION AVAILABLE

Description of the classical molecular dynamics protocol; Table S1 with atomic charges used in the MD simulations, Tables S2 and S3 with bonded force field parameters used in the MD simulations, Cartesian coordinates, and calculated energies for all ground and transition structures; Figure S1 showing the oxoferryl species with its first-shell ligands and atom names; Figure S2 showing atom types and charges used for PCA; Figure S3 showing a plot of rmsd vs time for the backbone atoms; Figure S4 presenting a plot of the critical (oxo)O−H(PCA) distances vs time; Figure S5, which shows a plot of the (PCA)O-H−O(oxo) angle vs time; Figures S6−S8 presenting the structures of species **c**, $\mathbf{TS}_{C-C}$, and $\mathbf{TS}_{C4-H-O}$, respectively. This material is available free of charge via the Internet at http://pubs.acs.org.

REFERENCES

1. Elson, S., Baggaley, K., Gillett, J., Holland, S., Nicholson, N., Sime, J., and Woroniecki, S. (1987) Isolation of two novel intracellular β-lactams and a novel dioxygenase cyclising enzyme from *streptomyces clavuligerus*, *J. Chem. Soc., Chem. Commun.*, 1736−1738.
2. Salowe, S., Marsh, E., and Townsend, C. (1990) Purification and characterization of clavaminate synthase from *streptomyces clavuligerus*: an unusual oxidative enzyme in natural product biosynthesis, *Biochemistry 29*, 6499−6508.
3. Baggaley, K., Brown, A., and Schofield, C. (1997) Chemistry and biosynthesis of clavulanic acid and other clavams, *Nat. Prod. Rep. 14*, 309−333.
4. Busby, R. W. and Townsend, C. A. (1996) A single monomeric iron center in clavaminate synthase catalyzes three nonsuccessive oxidative transformations, *Bioorg. Med. Chem. 4*, 1059−1064.
5. Khaleeli, N., Busby, R., and Townsend, C. (2000) Site-directed mutagenesis and biochemical analysis of the endogenous ligands in the ferrous active site of clavaminate synthase. The His-3 variant of the 2-His-1-carboxylate model, *Biochemistry 39*, 8666−8673.
6. Que, L. (2000) One motif−many different reactions, *Nat. Struct. Biol. 7*, 182−184.
7. Zhang, Z., Ren, J., Stammers, D., Baldwin, J., Harlos, K., and Schofield, C. (2000) Structural origins of the selectivity of the trifunctional oxygenase clavaminic acid synthase, *Nat. Struct. Biol. 7*, 127−133.
8. Schofield, C. and Zhang, Z. (1999) Structural and mechanistic studies on 2-oxoglutarate-dependent oxygenases and related enzymes, *Curr. Opin. Struct. Biol. 9*, 722−731.
9. Prescott, A. G. and Lloyd, M. D. (2000) The iron(II) and 2-oxoacid-dependent dioxygenases and their role in metabolism, *Nat. Prod. Rep. 17*, 367−383.
10. Pavel, E. G., Zhou, J., Busby, R. W., Gunsior, M., Townsend, C. A., and Solomon, E. I. (1998) Circular dichroism and magnetic circular dichroism spectroscopic studies of the non-heme ferrous active site in clavaminate synthase and its interaction with α-ketoglutarate cosubstrate, *J. Am. Chem. Soc. 120*, 743−753.
11. Zhou, J., Gunsior, M., Bachmann, B. O., Townsend, C. A., and Solomon, E. I. (1998) Substrate binding to the α-ketoglutarate-dependent non-heme iron enzyme clavaminate synthase 2: Coupling mechanism of oxidative decarboxylation and hydroxylation, *J. Am. Chem. Soc. 120*, 13539−13540.
12. Zhou, J., Kelly, W. L., Bachmann, B. O., Gunsior, M., Townsend, C. A., and Solomon, E. I. (2001) Spectroscopic studies of substrate interactions with clavaminate synthase 2, a multifunctional α-KG-dependent non-heme iron enzyme: Correlation with mechanisms and reactivities, *J. Am. Chem. Soc. 123*, 7388−7398.
13. Borowski, T., Bassan, A., and Siegbahn, P. E. M. (2004) Mechanism of dioxygen activation in 2-oxoglutarate-dependent enzymes: a hybrid DFT study, *Chem. Eur. J. 10*, 1031−1041.
14. Borowski, T., Bassan, A., and Siegbahn, P. E. M. (2004) 4-hydroxyphenylpyruvate dioxygenase: a hybrid density functional study of the catalytic reaction mechanism, *Biochemistry 43*, 12331−12342.
15. Price, J. C., Barr, E. W., Tirupati, B., Bollinger, J. M., and Krebs, C. (2003) The first direct characterization of a high-valent iron intermediate in the reaction of an α-ketoglutarate-dependent dioxygenase: a high-spin FeIV complex in taurine/alpha-ketoglutarate dioxygenase (TauD) from *Escherichia coli*, *Biochemistry 42*, 7497−7508.
16. Price, J. C., Barr, E. W., Glass, T. E., Krebs, C., and Bollinger, J. M. (2003) Evidence for hydrogen abstraction from C1 of taurine by the high-spin Fe(IV) intermediate detected during oxygen activation by taurine:α-ketoglutarate dioxygenase (TauD), *J. Am. Chem. Soc. 125*, 13008−13009.
17. Riggs-Gelasco, P. J., Price, J. C., Guyer, R. B., Brehm, J. H., Barr, E. W., Bollinger, J. M., and Krebs, C. (2004) EXAFS spectroscopic evidence for an Fe═O unit in the Fe(IV) intermediate observed during oxygen activation by taurine:alpha-ketoglutarate dioxygenase, *J. Am. Chem. Soc. 126*, 8108−8109.
18. Proshlyakov, D. A., Henshaw, T. F., Monterosso, G. R., Ryle, M. J., and Hausinger, R. P. (2004) Direct detection of oxygen intermediates in the non-heme Fe enzyme taurine/α-ketoglutarate dioxygenase, *J. Am. Chem. Soc. 126*, 1022−1023.
19. Baldwin, J., Merritt, K., Schofield, C., Elson, S., and Baggaley, K. (1993) Studies on the stereospecificity of the clavaminic acid synthase catalysed hydroxylation reaction, *J. Chem. Soc., Chem. Commun.*, 1301−1302.
20. Zhang, Z., Ren, J.-S., Harlos, K., McKinnon, C. H., Clifton, I. J., and Schofield, C. J. (2002) Crystal structure of a clavaminate synthase-Fe(II)-2-oxoglutarate-substrate-NO complex: evidence for metal centered rearrangements, *FEBS Lett. 517*, 7−12.
21. Humphrey, W., Dalke, A., and Schulten, K. (1996) VMD−Visual Molecular Dynamics, *J. Mol. Graphics 14*, 33−38.
22. Krol, W., Basak, A., Salowe, S., and Townsend, C. (1989) Oxidative cyclization chemistry catalyzed by clavaminate synthase, *J. Am. Chem. Soc. 111*, 7625−7627.
23. Baldwin, J., Adlington, R., Bryans, J., Bringhen, A., Coates, J., Crouch, N., Lloyd, M., Schofield, C., Elson, S., Baggaley, K., Cassells, R., and Nicholson, N. (1990) Isolation of an intermediate in clavulanic acid biosynthesis, *J. Chem. Soc., Chem. Commun.*, 617−619.
24. Basak, A., Salowe, S., and Townsend, C. (1990) Stereochemical course of the key ring-forming reactions in clavulanic acid biosynthesis, *J. Am. Chem. Soc. 112*, 1654−1656.
25. Salowe, S., Krol, W., Iwata-Reuyl, D., and Townsend, C. (1991) Elucidation of the order of oxidations and identification of an intermediate in the multistep clavaminate synthase reaction, *Biochemistry 30*, 2281−2292.
26. Iwata-Reuyl, D., Basak, A., and Townsend, C. (1999) β-Secondary kinetic isotope effects in the clavaminate synthase-catalyzed

oxidative cyclization of proclavaminic acid and in related azetidione model reactions, *J. Am. Chem. Soc. 121*, 11356−11368.
27. Case, D. A., Darden, T. A., Cheatham, T. E., III, Simmerling, C. L., Wang, J., Duke, R. E., Luo, R., Merz, K. M., Wang, B., Pearlman, D. A., Crowley, M., Brozell, S., Tsui, V., Gohlke, H., Mongan, J. Hornak, V., Cui, G., Beroza, P., Schafmeister, C., Caldwell, J. W., Ross, W. S., and Kollman, P. A. (2004) *AMBER 8*, University of California, San Francisco, CA.
28. Becke, A. D. J. (1993) Density-functional thermochemistry. III. The role of exact exchange, *Chem. Phys. 98*, 5648−5652.
29. Lee, C., Yang, W., and Parr, R. G. (1988) Development of the Colle-Salvetti correlation energy formula into a functional of the electron density, *Phys. Rev. B* 37, 785−789.
30. Schrödinger, Inc. (2005) *JAGUAR 5.5*, Portland, OR.
31. Tannor, D. J., Marten, B., Murphy, R., Friesner, R. A., Sitkoff, D., Nicholls, A., Ringnalda, M., Goddard, W. A., III, and Honig, B. (1994) Accurate first principles calculation of molecular charge distributions and solvation energies from ab initio quantum mechanics and continuum dielectric theory, *J. Am. Chem. Soc. 116*, 11875−11882.
32. Marten, B., Kim, K., Cortis, C., Friesner, R. A., Murphy, R., Ringnalda, M., Sitkoff, D., and Honig, B. (1996) New model for calculation of solvation free energies: correction of self-consistent reaction field continuum dielelectric theory for short-range hydrogen-bonding effects, *J. Phys. Chem. 100*, 11775−11788.
33. Viehe, H. G., Janousek, Z., Merenyi, R., and Stella, L. (1985) The captodative effect, *Acc. Chem. Res. 18*, 148−154.
34. Ess, D. H., and Houk, K. N. (2005) Activation energies of pericyclic reactions: performance of DFT, MP2, and CBS-QB3 methods for the prediction of activation barriers and reaction energetics of 1,3-dipolar cycloadditions, and revised activation enthalpies for a standard set of hydrocarbon pericyclic reactions, *J. Phys. Chem. A 109*, 9542−9553.
35. Brown, D., Brown, G. A., Martel, S. R., Planchenault, D., Turmes, E., Walsh, K. E., Wisedale, R., Hales, N. J., Fishwick, C. W. G., and Gallagher, T. (2001) The azomethine ylide strategy for β-lactam synthesis. A comprehensive mechanistic evaluation, *J. Chem. Soc., Perkin Trans. 1*, 1270−1280.
36. Brown, G. A., Martel, S. R., Wisedale, R., Charmant, J. P. H., Hales, N. J., Fishwick, C. W. G., and Gallagher, T. (2001) The azomethine ylide strategy for β-lactam synthesis. An evaluation of alternative pathways for azomethine ylide generation, *J. Chem. Soc., Perkin Trans. 1*, 1281−1289.
37. Martel, S. R., Wisedale, R., Gallagher, T., Hall, L. D., Mahon, M. F., Bradbury, R. H., and Hales, N. J. (1997) β-Lactam-based azomethine ylide reactivity. Expedient synthesis of carbapenams and carbapenems, *J. Am. Chem. Soc. 119*, 2309−2310.
38. Andrews, M. D., Brown, G. A., Charmant, J. P. H., Peakman, T. M., Rebello, A., Walsh, K. E., Gallagher, T., and Hales, N. J. (1999) Aldehydes and ketones as dipolarophiles: application to the synthesis of oxapenams, *Chem. Commun*., 249−250.
39. Lewis, W. G., Green, L. G., Grynszpan, F., Radic, Z., Carlier, P. R., Taylor, P., Finn, M. G., and Sharpless, K. B. (2002) Click chemistry in situ: acetylcholinesterase as a reaction vessel for the selective assembly of a femtomolar inhibitor from an array of building blocks, *Angew. Chem., Int. Ed.*, 1053−1057.
40. van Lier, J. E. and Rousseau, J. (1976) Mechanism of cholesterol side-chain cleavage: enzymic rearrangement of 20β-hydroperoxy-20-isocholesterol to 20β,21-dihydroxy-20-isocholesterol, *FEBS Lett. 70*, 23−27.
41. Borowski, T., and Broclawik, E. (2003) Catalytic reaction mechanism of lipoxygenase. A density functional theory study, *J. Phys. Chem. B 107*, 4639−4646.
42. Rétey, J. (1990) Enzymic reaction selectivity by negative catalysis or how do enzymes deal with highly reactive intermediates?, *Angew. Chem., Int. Ed. 29*, 355−361.

BI602458M